MASSACHUSETTS INSTITUTE OF TECHNOLOGY
HAYSTACK OBSERVATORY
WESTFORD, MASSACHUSETTS 01886
February 10, 2020

Telephone: 617-715-5517
Fax: 617-715-0590

To: IVS VGOS Correlation Groups

From: J. Barrett, R. Cappallo, B. Corey, P. Elosegui, D. Mondal, A. Niell, C. Ruszczyk, and M. Titus

Subject: Comparison of correlator results from VGOS VO0009

1 Introduction

A blind test involving several correlation centers and using data from the intensive session VI9290 uncovered several parts of the VGOS data processing pipeline where the results of each correlation center diverged from one another([1]). Notably, the most problematic parts identified during that exercise were found to be:

1. Corruption of data during e-transfer.
2. The determination of the correlator clock model.
3. The construction of an initial-pass fourfit control to be used when generating a calibrated production-pass fourfit control file.
4. The selection of the appropriate band/polarizations for use when generating proxy cable-calibration delay files.

These discoveries lead to some changes to post-processing software (updated to HOPS 3.22) and have guided the manner in which the second test has been done. In order to verify that we have the correct understanding of the issues encountered in the first blind test, a follow-up exercise has been performed, in which the correlator clock model has been provided, as well as an initial control file together with instructions on the generation of the proxy cable-calibration delays. Furthermore, for this second test the data set has been enlarged to a full 24-hour VGOS session with six stations.

To show that two separate correlators can obtain equivalent results when given the same data and data processing procedure we have divided this exercise into two parts. The first part of this test was intended to validate solely the post-correlation portion of the VGOS data processing pipeline and was executed by WACO, Vienna, and Shanghai on a set of pre-correlated (by Haystack) data. The second portion of this test was intended to confirm the full data processing chain, from correlation of the raw data through post-processing and was executed by Bonn. However, it should be stressed that the process of setting the correlator clock model has not been considered in this exercise, but is a critical part of the correlation process which needs to be addressed and specified in the near future.

2 Methods

The first portion of this test was primarily intended as a quick verification of the post-processing software and the correlation centers, to ensure they can obtain consistent results when used in the same way. To this end HOPS 3.22 was distributed along with pre-correlated data in the form of DiFX output binary files. The participating correlators (WACO, Vienna, and Shanghai) were then tasked with performing the following:

1. E-transfer the DiFX output files from Haystack.
2. Convert the DiFX binaries into the Mark4-type format for processing with HOPS using difx2mark4.
3. Use the provided initial control file to run vgoscf_generate.py to produce the production fourfit control file.
4. Batch fourfit the data of the entire session.
5. Run the proxy cable-calibration delay generation script and use the provided band-pol selection to create the delay files.

6. Create a vgosDb database and apply the proxy cable-calibration delays.

The second portion of this test was carried by Bonn and consisted of the following:

1. Receive the Mark6 modules for session vo0009 from Haystack.
2. Use the provided Haystack clock model and .vex template to set up DiFX correlation (using version 2.5.3).
3. Correlate the session and use difx2mark4 to convert the DiFX output to mark4 types.
4. Using the provided initial control file, run vgoscf_generate.py to produce the production fourfit control file
5. Batch fourfit the data of the entire session.
6. Run the proxy cable-calibration delay generation script and use the provided band-polarization selection to create the delay files.
7. Create a vgosDb database and apply the proxy cable-calibration delays.

The resulting output from these exercises were then returned to Haystack for analysis.

3 Results

To compare the results generated by each correlation center we examined the the following set of parameters and compared them to the values obtained by Haystack. These were:

1. The Y-X polarization phase and delay offsets, and the applied pc_phases in the control file for each station-polarization.
2. The SNR of each scan-baseline.
3. The residual multi-band delay of each scan-baseline.
4. The differential total electron content (dTEC) of each scan-baseline.
5. Total multi-band delay of each scan-baseline.
6. The proxy cable-calibration delays.

3.0.1 Control file parameters

The station parameters of the production fourfit control files for all of the participating correlations center are shown in tables 1 and 2 and figures (1a) through (6b). Table 1 shows the Y-X polarization delay offsets derived for each station, while 2 shows the Y-X polarization phase offsets. For all correlations centers the derived values of the delay and phase offsets for each station are consistent with each other to within the estimated errors or better. Figures (1a) through (6b) show the manual per-channel phase-cal offsets (pc_phases) derived by each correlation center as applied to both polarizations of each the station involved in vo0009. By and large the pc_phases derived by each correlation center are consistent with each other to within $\sim$5 degrees or better, and upon closer examination it should be noted that the pc_phases derived by Vienna and WACO match Haystack's values exactly.

3.0.2 Vienna and WACO

The results obtained by Vienna and WACO from the post-processing exercise are identical to those which were obtained by Haystack. This can be seen at all stages of the post-processing, including the control file parameters, the total-multi-band delay computed for each scan-baseline, as well as the proxy cable-calibration delays. In figures 9f and 10f it can be seen that the differences in the total multi-band delay with respect to Haystack are essentially zero.

3.0.3 Shanghai

The results obtained by Shanghai are slightly different from Haystack's results. The reason for this is due to the inclusion of one additional station (McDonald Geodetic Observatory, MGO) during the post-processing step of generating the production fourfit control file, which affected some of the parameters applied to the network reference station GGAO12M. During session vo0009, MGO was participating as a tag-a-long station, which had not yet been fully vetted. For this reason, we decided to exclude the MGO data (as well as Yebes which at the time was using an experimental 10MHz phase-cal. system) from this correlation exercise. However, due to the fact that the pre-correlated data was e-transferred in the form of DiFX output files, it was not possible to separate out data specific to these two stations.

Why would the inclusion of MGO affect the control file parameters applied to GGAO12M? This is due to the manner in which the Y-X phase and delay offsets (as well as the Y-polarization pc_phases) are derived for the network phase reference station (GGAO12M), which uses data involving all of the other participating stations. Since the X-polarization at GGAO12M serves as the network phase-reference, and for all other stations in the network, computing the X or Y pc_phases must be derived from fringes involving G:X. However, there is no direct way to compute the pc_phases for G:Y, because while it might in theory be possible to use the cross-auto-correlation products (G:X to G:Y), these data are highly contaminated by phase-calibration tones. Therefore the only way to compute the s associated with G:Y is indirectly via another intermediate station. This is done by calculating the differences of the phase residuals for a good quality fringe for the pol-products (XX - YX) or (XY - YY) on a baseline where 'G' is the reference station. These differences are then averaged over multiple baselines and sources. Including MGO in the data-set adds extra data to this average and introduces slight changes in the resulting Y-polarization pc_phases derived for GGAO12M.

Fortunately however, these differences in Shanghai's results are for the most part very small, and with the exception of two scans, all of total multi-band delays obtain by Shanghai agree with the Haystack results to within one picosecond. The two scans which do not agree to within one picosecond (visible in figures 11e and 11f), are due to observations which exhibit zero-fringe rate and have been flagged with error code 'G' to be discarded.

3.0.4 Bonn

The test exercise carried out by Bonn included not only the post-processing portion of the data pipeline but also the correlation of the raw data. Unsurprisingly, this additional processing step results in somewhat larger differences between Bonn's total multi-band delay and Haystack's than seen with the other correlation centers which used pre-correlated data. In figure 8 subtle differences in the SNR of each scan-baseline between Bonn and Haystack are visible. Upon further inspection the reason for this is apparently shorter correlation integration time for some observations at Bonn, which is likely caused by problems with playback from one or more modules. These slight changes in SNR also caused the derived station pc_phases to diverge slightly (as is visible in figures 1a) through (6b), which tend to bias the total multi-band delay of each scan-baseline away from Haystack's value. The broader distribution in $\Delta\tau_{MBD}$ is visible in figure 12c, not that there are approximately 100 scans with $|\Delta\tau_{MBD}|$ between 2-6 picoseconds which are not visible on the vertical (linear) scale of the histogram. However, it should be noted that the vast majority of observations (7980 out of 8168) correlated by Bonn exhibit a difference in the total multi-band delay (from the Haystack value) which is less then two picoseconds. There is however a small fraction (<0.4%) of scans which have drastically higher differences in the total multi-band-delay. Table 3 provides details on the most egregious examples. The worst offenders (having $\Delta\tau_{MBD}$ of thousands of picoseconds) are almost entirely due to observations which are flagged a non-detections (fringe quality of '0') or exhibit some other error (e.g. a 'G' code). However, there are still a handful of scans which exhibit $\Delta\tau_{MBD}$ in the hundreds of picoseconds that are not otherwise flagged as bad data. The root cause for these differences is not readily apparent, though it should be noted that they are also highly correlated with large differences in the estimated differential total electron content (dTEC). In some cases (especially for low SNR observations) we suspect that this might be explained by the differences in the correlator integration time, as this could introduce additional phase noise that might cause fourfit's minimization algorithm to locate a different solution. However, there does not appear to be a particularly strong correlation between $\Delta\tau_{MBD}$ and the difference in correlator integration time. This can be seen in figure 13 which shows a plot of the logarithm of $\Delta\tau_{MBD}$ as a function of the difference in correlator integration time. Furthermore, there are at least five observations which exhibit no difference in correlator integration time but which still exhibit a large value of $\Delta\tau_{MBD}$ in the hundreds of picoseconds (though they were assigned low quality codes). Incidentally, most of these problematic observations are associated with only a handful of sources (3C418, 0642+449, 1418+546, and 1406-076), which leads us to speculate that source structure might play some role in these discrepancies (perhaps by introducing non-linear phase structure across the four observing bands which makes it difficult to reliably determine the dTEC).

3.1 Proxy cable-calibration

Among the several correlation centers the differences in the proxy cable-calibration delay of the stations for which it was applied (GGAO12M, Ishioka, and Wettzell) were negligible, generally speaking being much less than 1

picosecond. This is simply due to the fact that all the correlation centers were instructed to use the same set of band-polarizations over which to average the proxy cable-calibration delay.

4 Conclusion

A comparison of the results of several correlation centers using data from VGOS session vo0009 was done in two parts in order to test the correlation and post-processing. In the case of Vienna and WACO, little to no differences were found in their results as compared with Haystacks. For Shanghai some slight differences in the total multi-band delay were found (< 1 picosecond), and the cause was determined to be changes in the control file parameters introduced by the inclusion of MGO data (nominally excluded for the purpose of this test). Bonn not only executed the post-processing exercise but also correlated the raw data and (at least in regard to the total multi-band delay of each observation) obtained results which were quite close to Haystack's, with 97.7% of all observations exhibiting $\Delta\tau_{MBD} < 2$ picoseconds. However, there was some loss of data due to playback issues at Bonn which lead to some observations having the total correlator integration time reduced by several seconds. This (relatively small) data loss is likely to be the main contributing cause to the majority of the observed differences. However, there are a handful of observations which do not appear to suffer from any data loss, but which nevertheless exhibit large differences (100s of picoseconds) in the total multi-band delay. We expect that it is likely that observations of the type which have exhibited large $\Delta\tau_{MBD}$ in this study may be rejected as outliers in the normal course of further geodetic analysis by downstream tools (e.g. nuSolve) but this requires further investigation to be verified.

References

[1] J. Barrett, R. Cappallo, B. Corey, P. Elosegui, D. Mondal, A. Niell, C. Ruszczyk, and M. Titus. Comparison of correlator results from vgos intensive vi9290 test, 20209. URL: `https://www.haystack.mit.edu/geo/vlbi_td/BB/051.pdf`.

[2] I Boris and D Hoaglin. How to Detect and Handle Outliers, the ASQC Basic References in Quality Control: Statistical Techniques, 1993.

Station Quantity	Haystack	Bonn	Vienna	WACO	Shanghai
(G) Gs Y-X delay offset (ns)	1.683 ± 0.002	1.683 ± 0.002	1.683 ± 0.002	1.683 ± 0.002	1.683 ± 0.002
(E) Wf Y-X delay offset (ns)	0.731 ± 0.003	0.731 ± 0.002	0.731 ± 0.003	0.731 ± 0.003	0.730 ± 0.003
(I) Is Y-X delay offset (ns)	-0.061 ± 0.002	-0.061 ± 0.002	-0.061 ± 0.002	-0.061 ± 0.002	-0.061 ± 0.002
(S) Oe Y-X delay offset (ns)	-0.109 ± 0.002	-0.109 ± 0.002	-0.109 ± 0.002	-0.109 ± 0.002	-0.109 ± 0.003
(T) Ow Y-X delay offset (ns)	0.215 ± 0.004	0.215 ± 0.004	0.215 ± 0.004	0.215 ± 0.004	0.215 ± 0.004
(V) Ws Y-X delay offset (ns)	-0.058 ± 0.002	-0.058 ± 0.002	-0.058 ± 0.002	-0.058 ± 0.002	-0.058 ± 0.002

Table 1: Y-X polarization delay offsets set for each station by correlator.

Station Quantity	Haystack	Bonn	Vienna	WACO	Shanghai
(G) Gs Y-X phase offset (deg)	36.0 ± 3.5	36.1 ± 3.3	36.0 ± 3.5	36.0 ± 3.5	35.8 ± 3.3
(E) Wf Y-X phase offset (deg)	129.1 ± 3.8	129.4 ± 3.7	129.1 ± 3.8	129.1 ± 3.8	128.9 ± 3.7
(I) Is Y-X phase offset (deg)	41.0 ± 4.1	41.0 ± 4.2	41.0 ± 4.1	41.0 ± 4.1	41.0 ± 4.0
(S) Oe Y-X phase offset (deg)	121.0 ± 4.4	121.4 ± 4.5	121.0 ± 4.4	121.0 ± 4.4	120.5 ± 4.7
(T) Ow Y-X phase offset (deg)	-64.4 ± 7.7	-64.0 ± 7.7	-64.4 ± 7.7	-64.4 ± 7.6	-65.3 ± 7.8
(V) Ws Y-X phase offset (deg)	-134.1 ± 4.9	-133.9 ± 4.8	-134.1 ± 4.9	-134.1 ± 4.9	-134.1 ± 4.5

Table 2: Y-X polarization phase offsets set for each station by correlator.

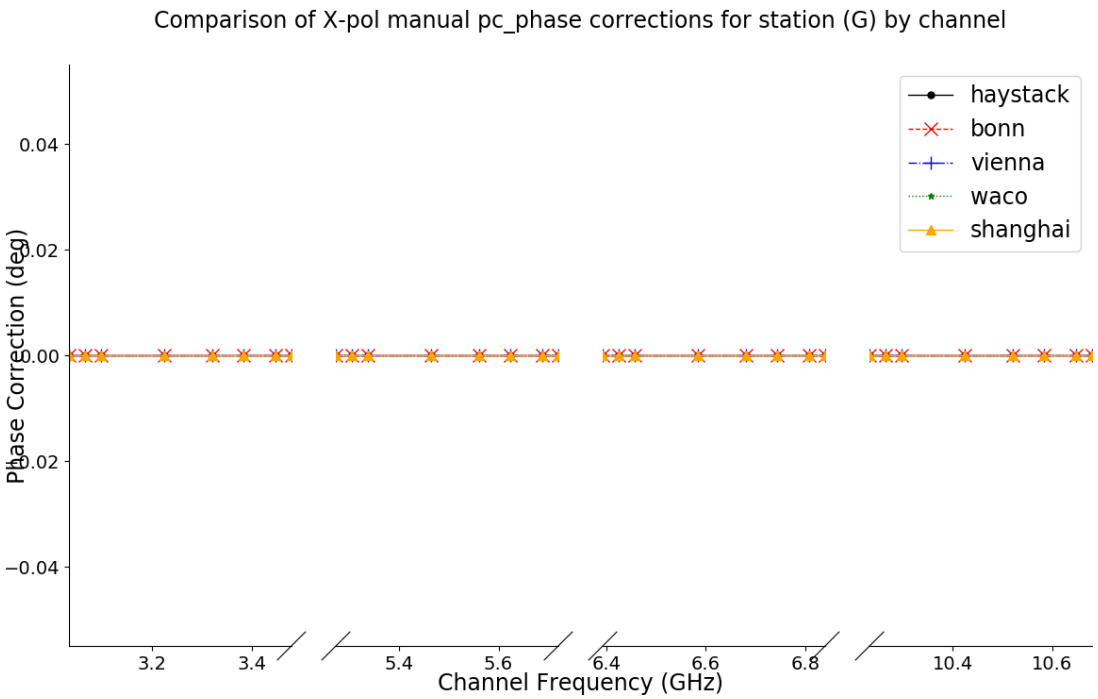

(a) X-polarization pc_phases for station G.

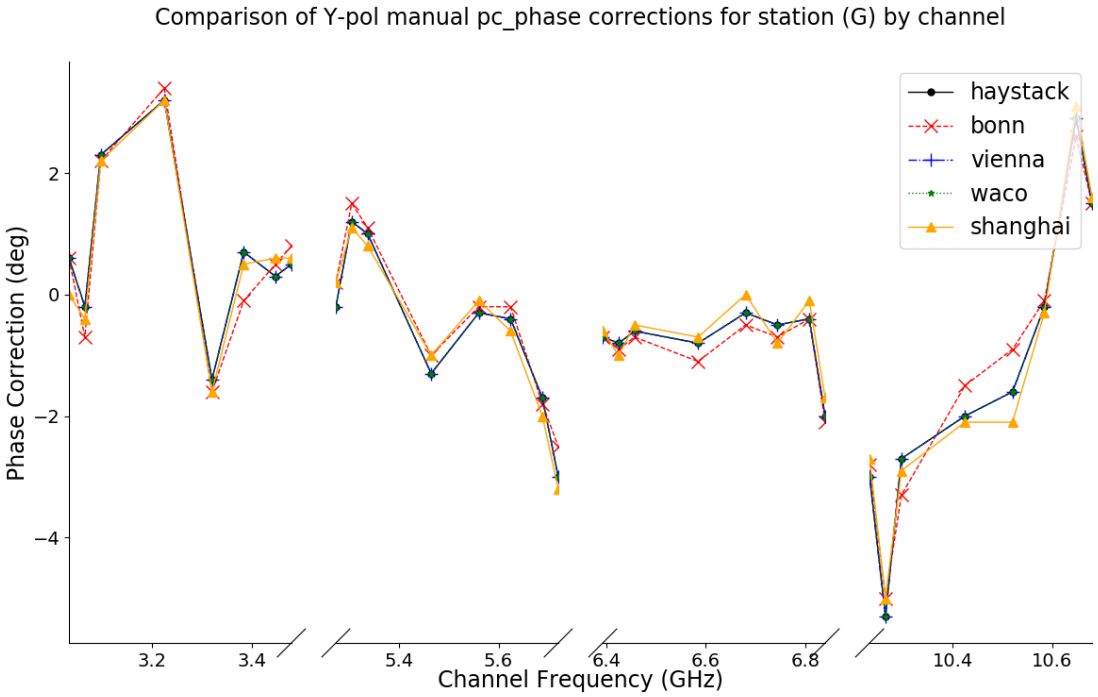

(b) Y-polarization pc_phases for station G.

Figure 1: Comparison of control file parameters for each correlator of station G (GGAO12M).

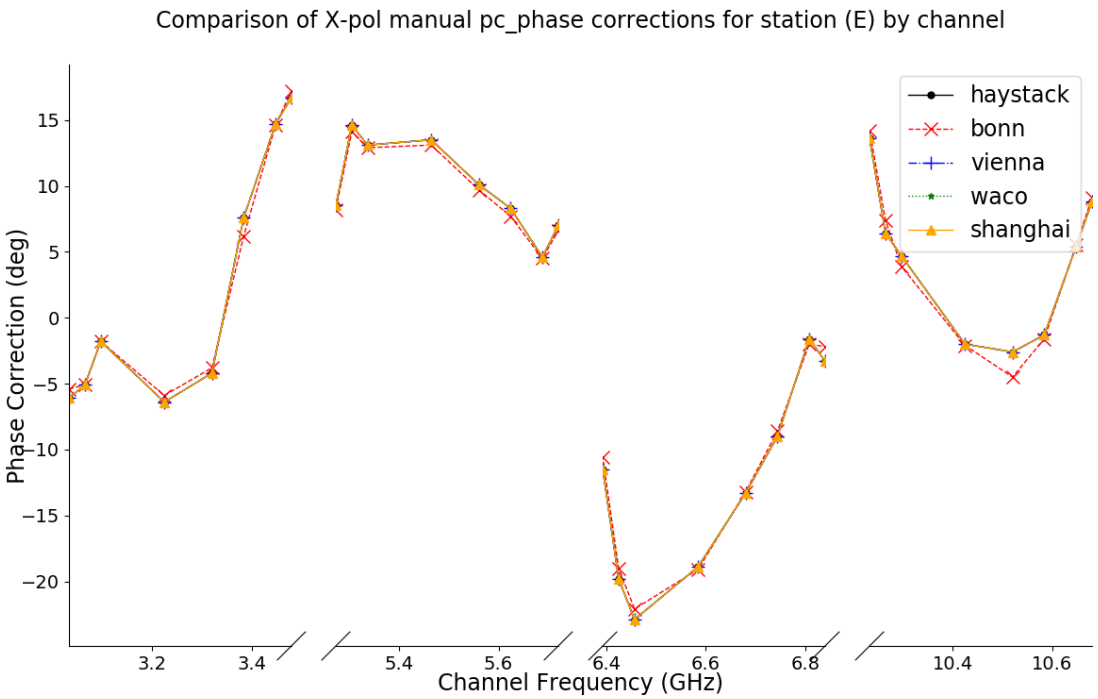

(a) X-polarization pc_phases for station E.

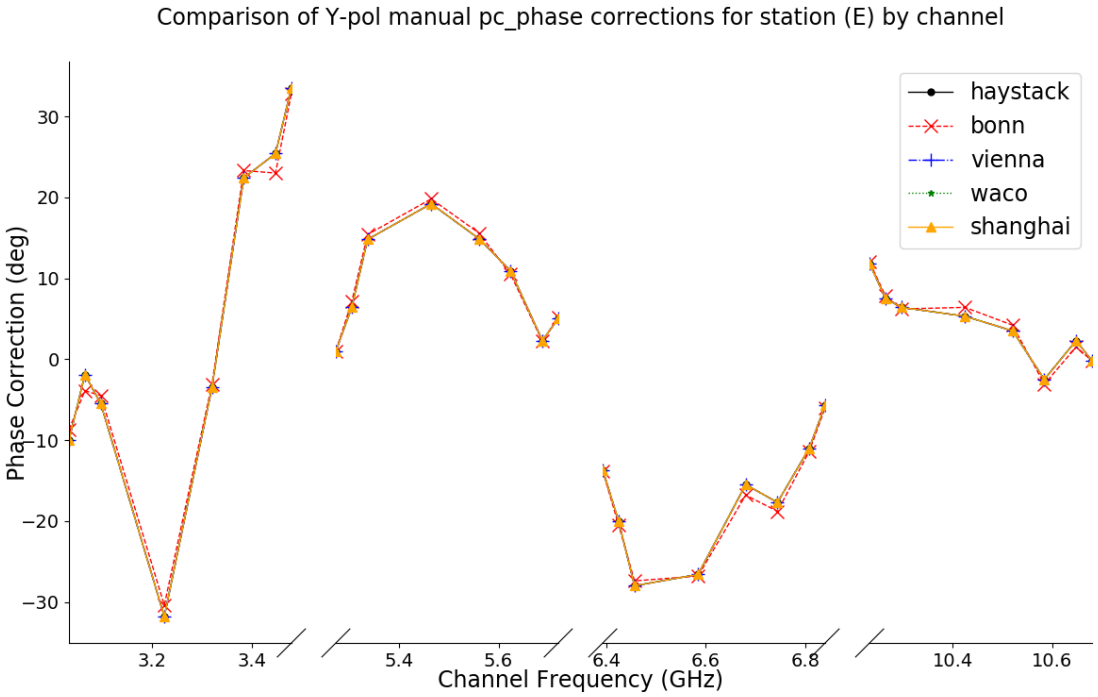

(b) Y-polarization pc_phases for station E.

Figure 2: Comparison of control file parameters for each correlator of station E (WESTFORD).

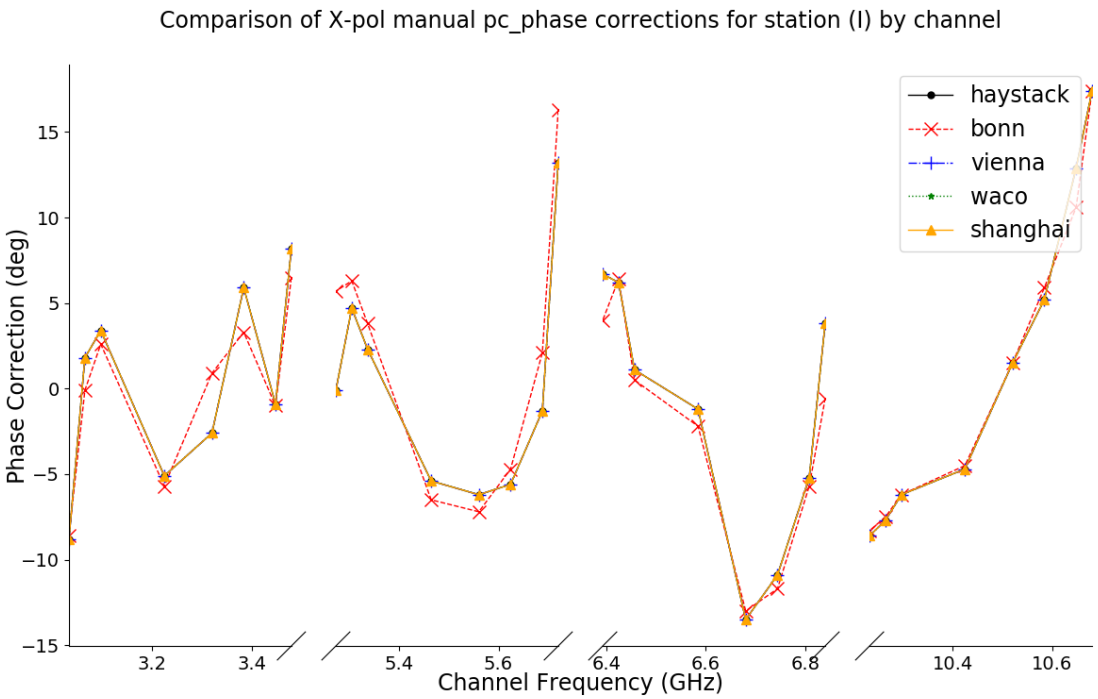

(a) X-polarization pc_phases for station I.

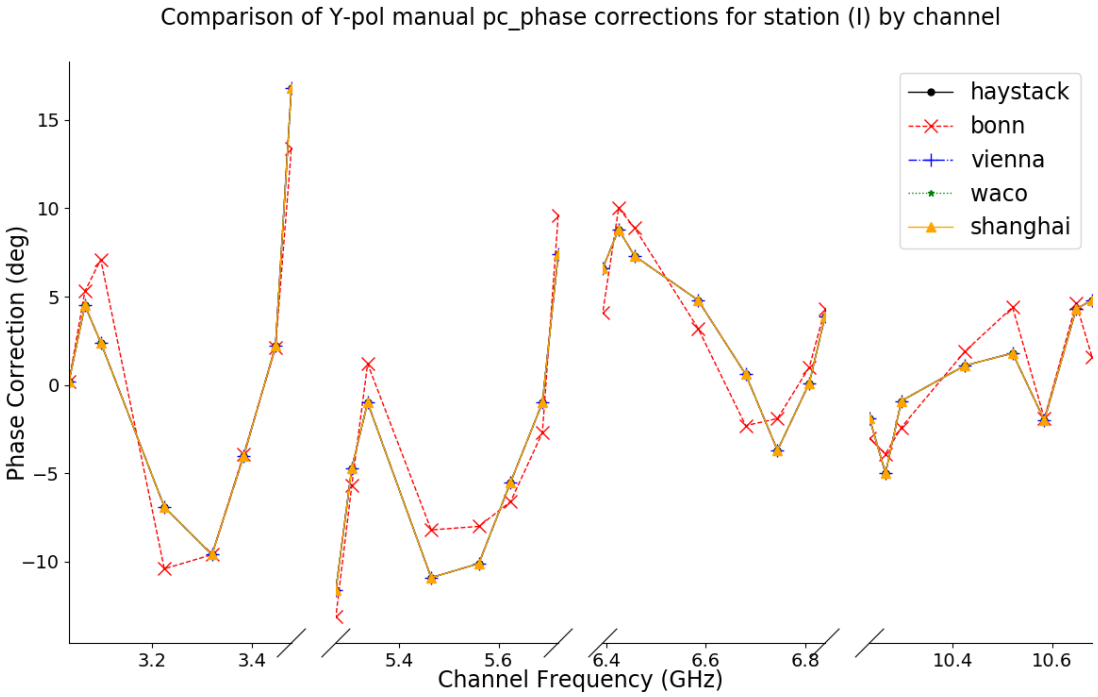

(b) Y-polarization pc_phases for station I.

Figure 3: Comparison of control file parameters for each correlator of station I (ISHIOKA).

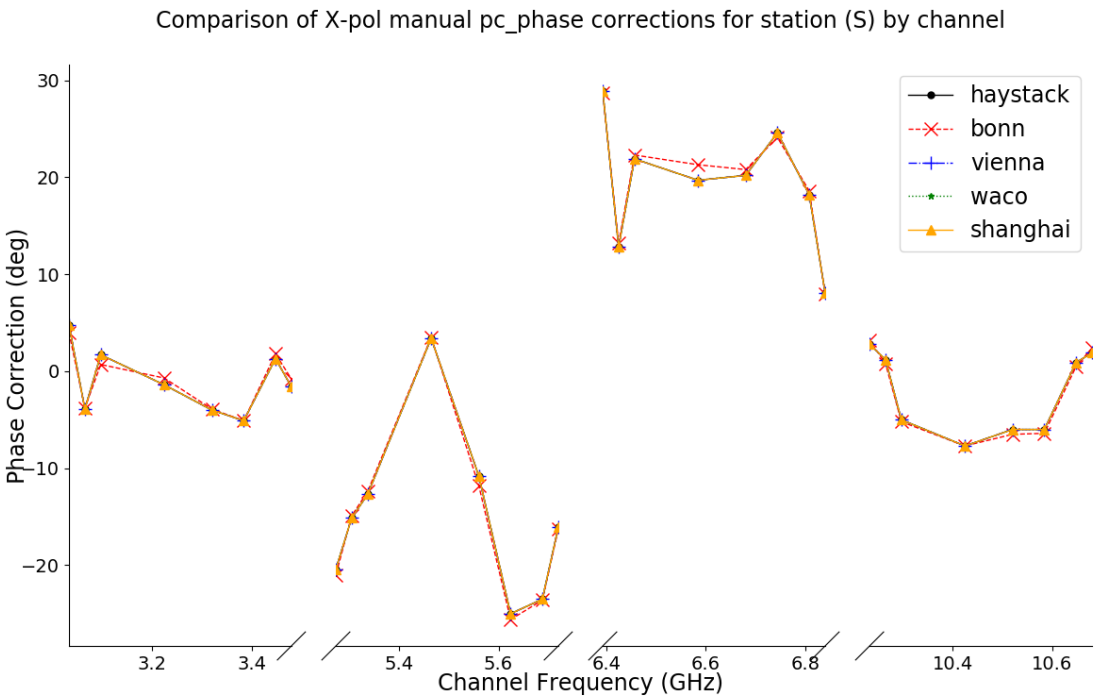

(a) X-polarization pc_phases for station S.

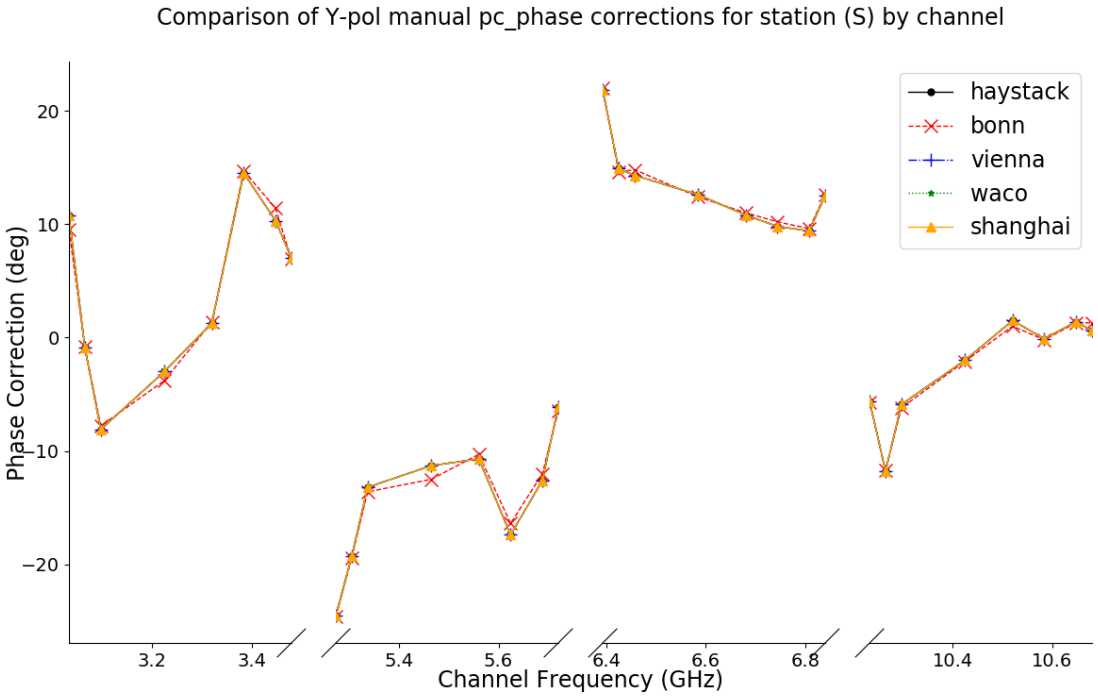

(b) Y-polarization pc_phases for station S.

Figure 4: Comparison of control file parameters for each correlator of station S (ONSA13NE).

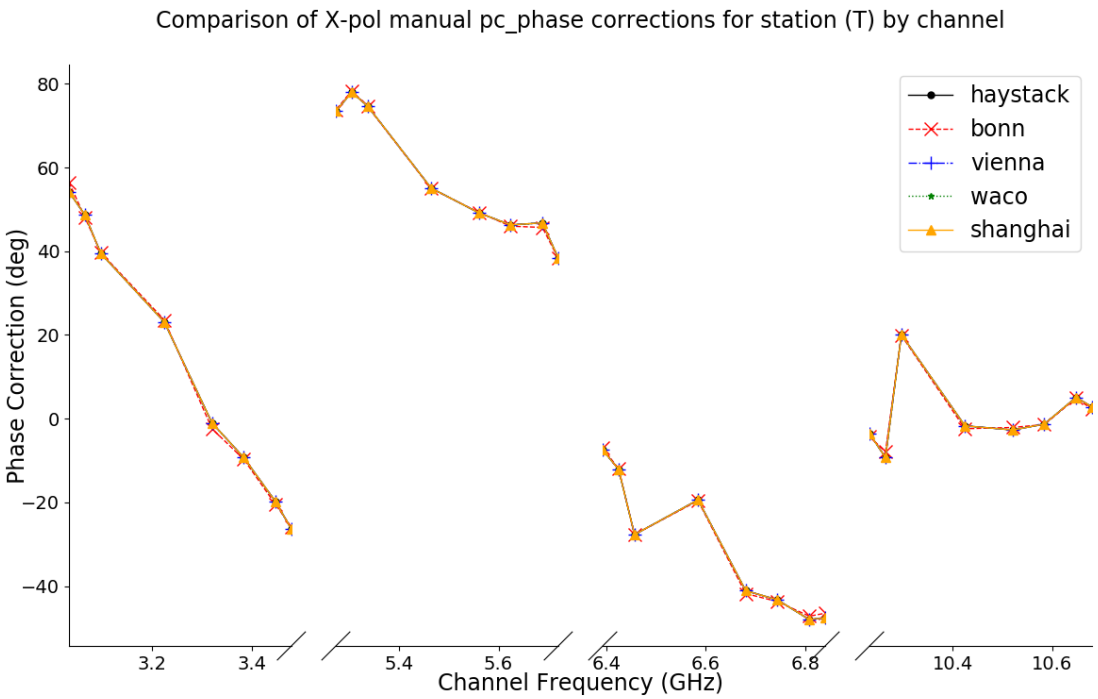

(a) X-polarization pc_phases for station T.

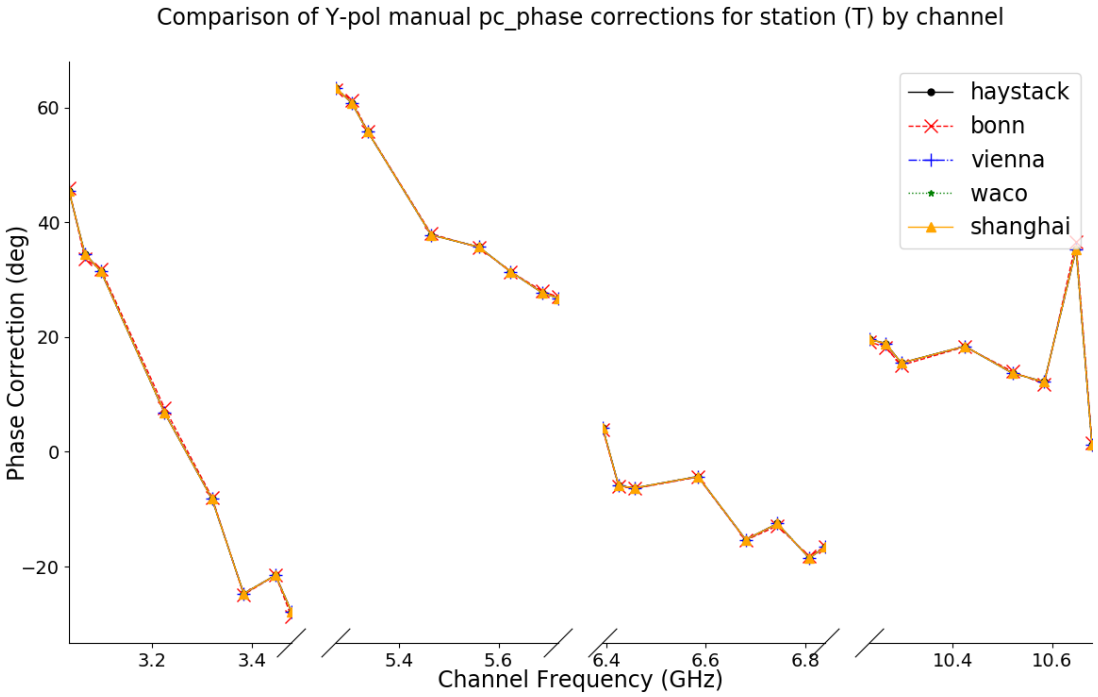

(b) Y-polarization pc_phases for station T.

Figure 5: Comparison of control file parameters for each correlator of station T (ONSA13SW).

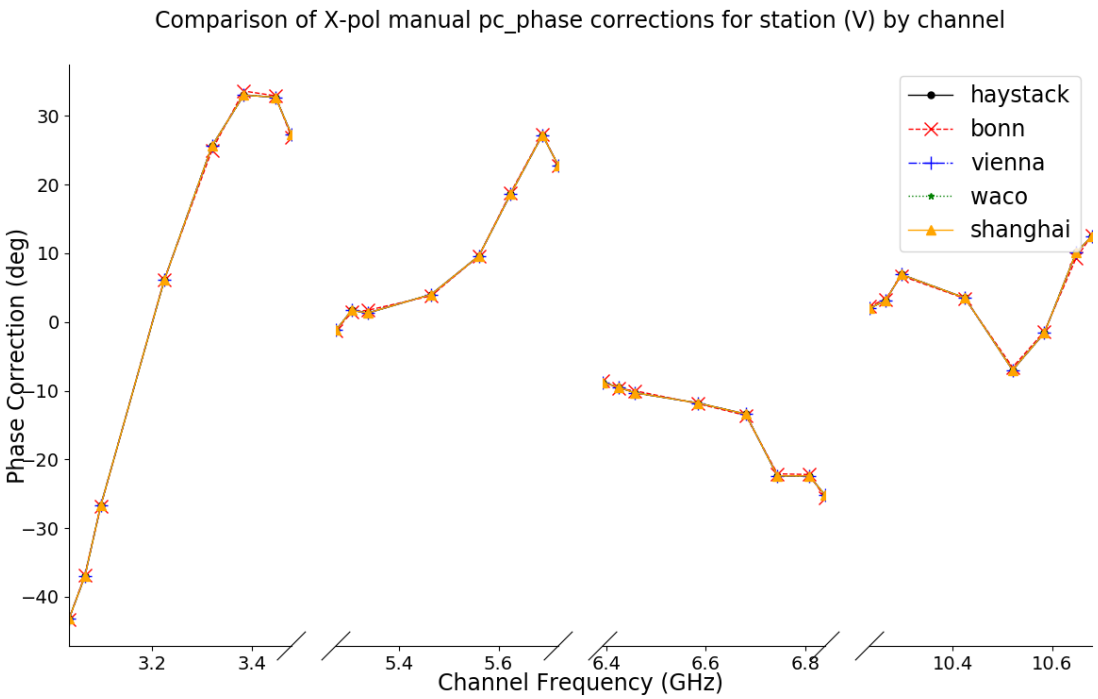

(a) X-polarization pc_phases for station V.

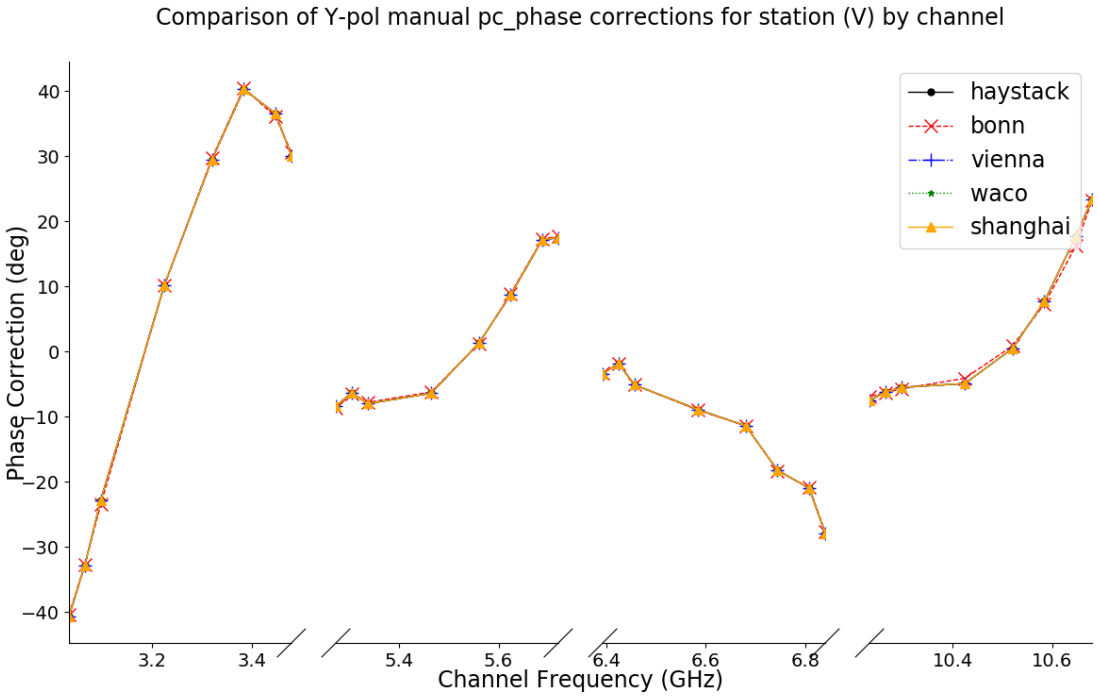

(b) Y-polarization pc_phases for station V.

Figure 6: Comparison of control file parameters for each correlator of station V (WETTZ13S).

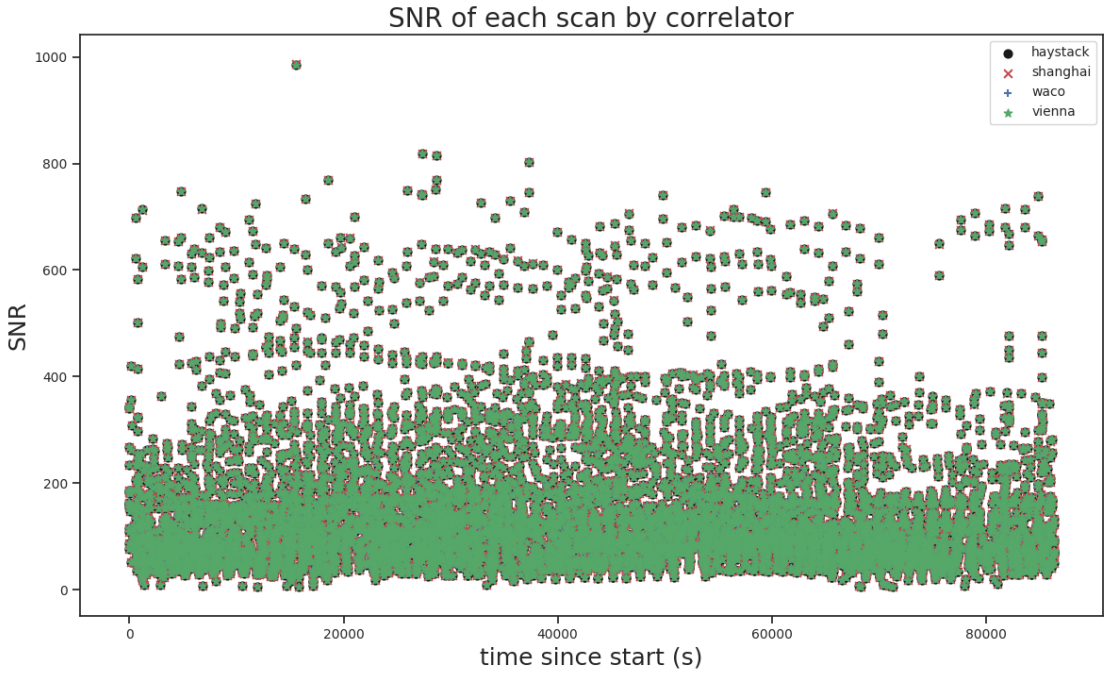

Figure 7: Plot of the SNR of each scan-baseline produced by the correlation centers Vienna, WACO and Shanghai as compared to Haystack.

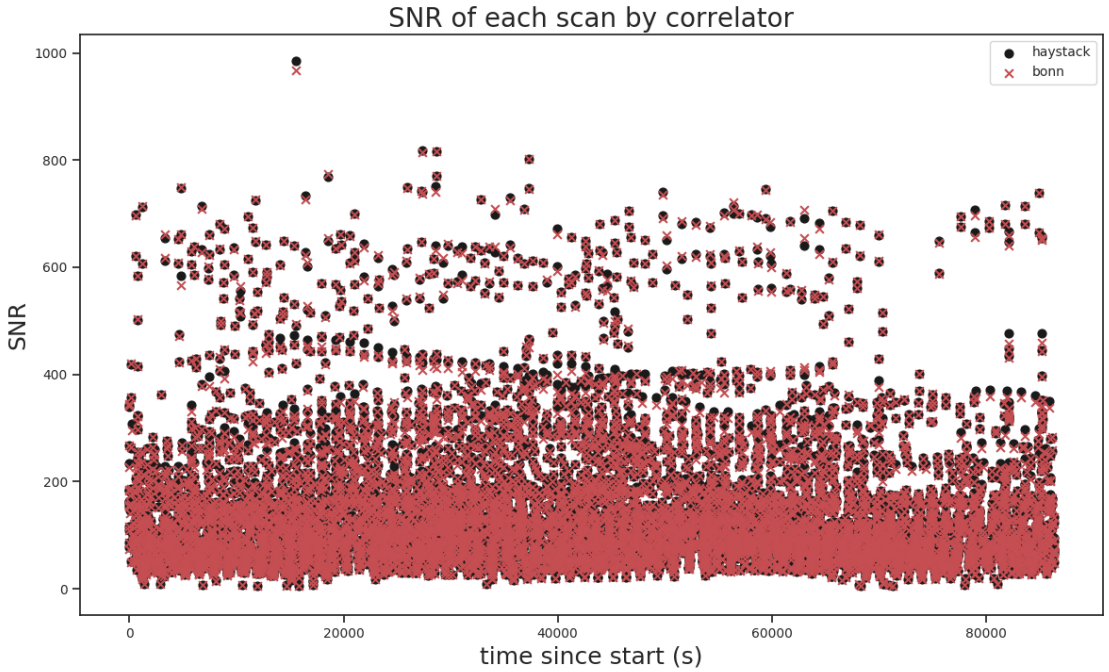

Figure 8: Plot of the SNR of each scan-baseline as produced by Bonn and Haystack.

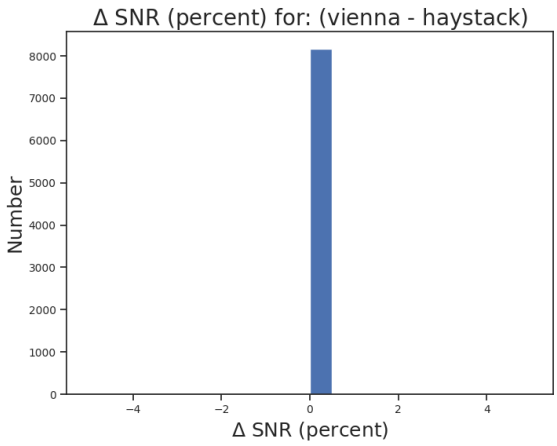

(a) Distribution of the difference in scan SNR

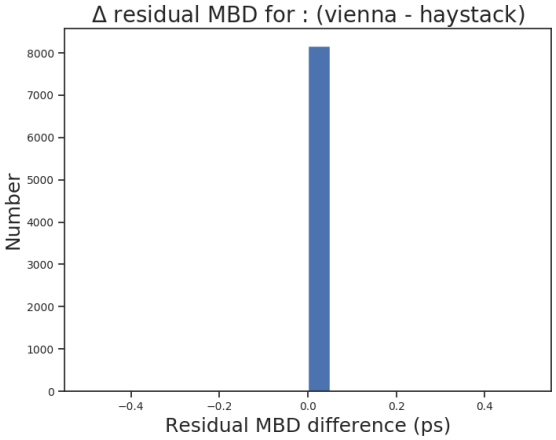

(b) Distribution of the difference in residual multi-band delay

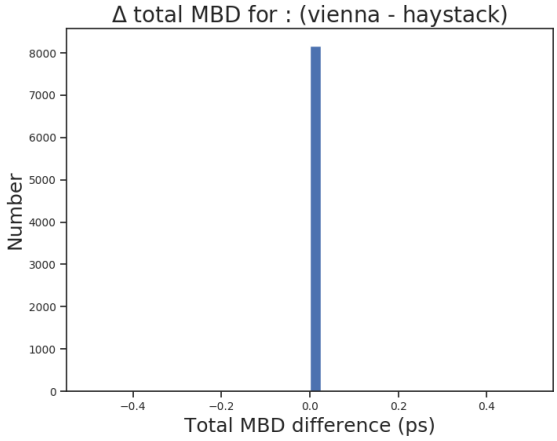

(c) Distribution of the difference in the total multi-band delay

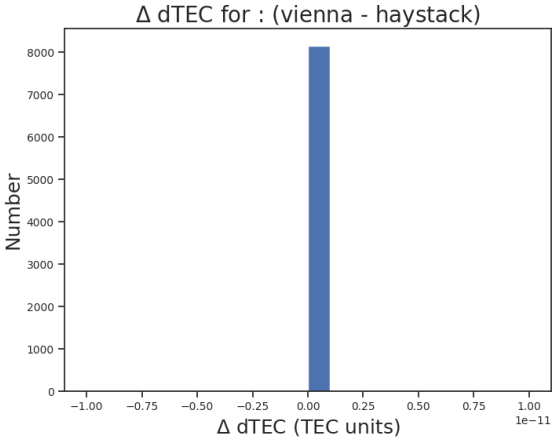

(d) Distribution of the difference in the scan dTEC

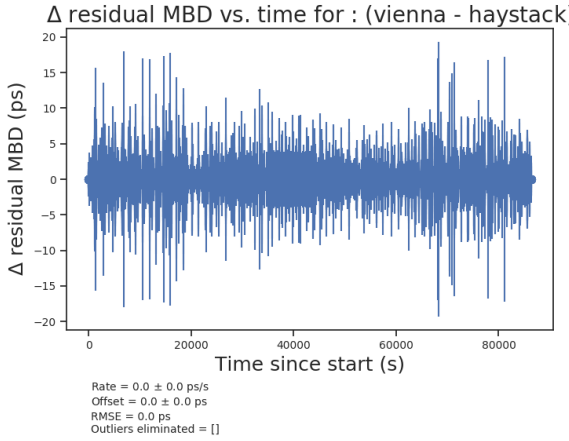

(e) Difference in the residual multi-band delay as a function of time since start, error bars are the formal MBD error reported by fourfit.

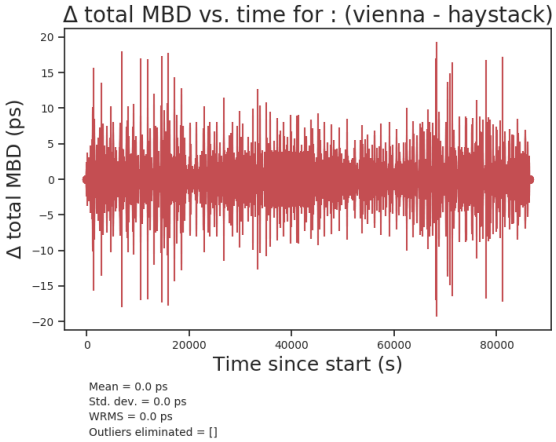

(f) Difference in the total multi-band delay as a function of time since start, error bars are the formal MBD error reported by fourfit.

Figure 9: Comparison of Vienna scan parameters with Haystack for vo0009

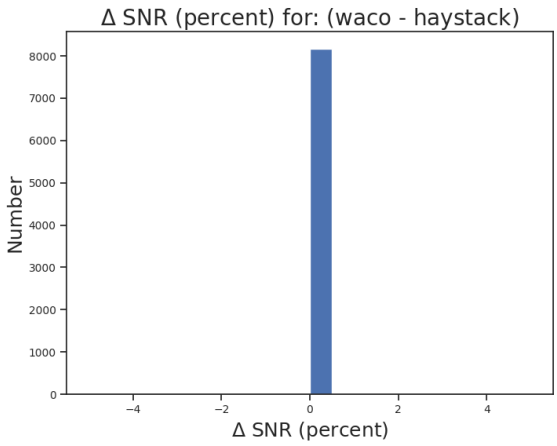

(a) Distribution of the difference in scan SNR

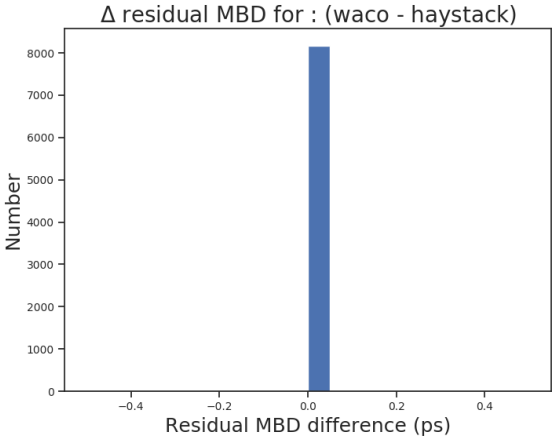

(b) Distribution of the difference in residual multi-band delay

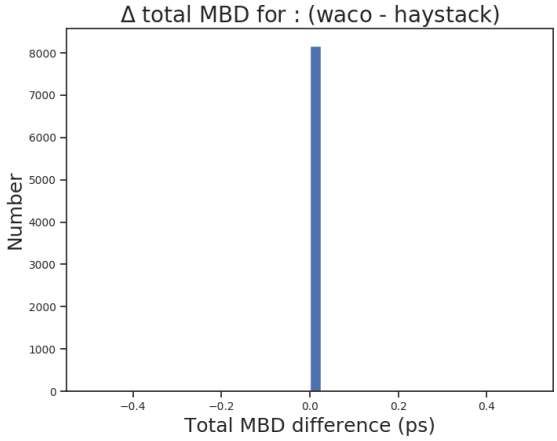

(c) Distribution of the difference in the total multi-band delay

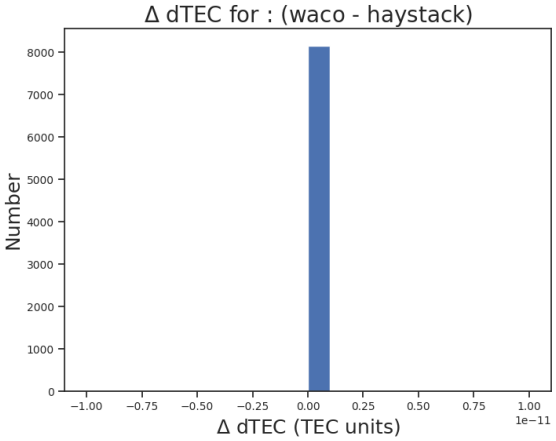

(d) Distribution of the difference in the scan dTEC

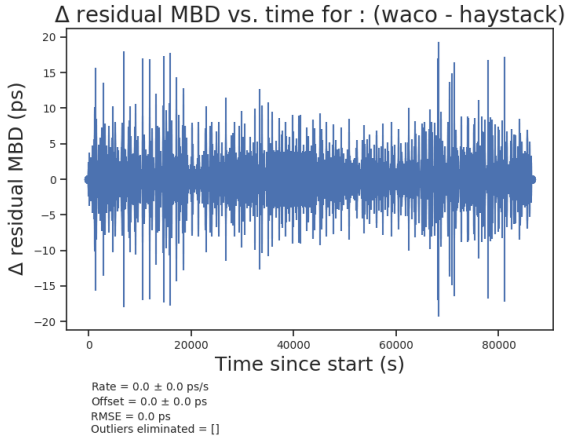

(e) Difference in the residual multi-band delay as a function of time since start, error bars are the formal MBD error reported by fourfit.

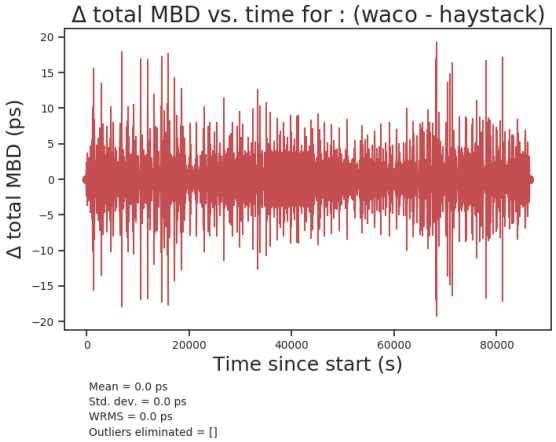

(f) Difference in the total multi-band delay as a function of time since start, error bars are the formal MBD error reported by fourfit.

Figure 10: Comparison of WACO scan parameters with Haystack for vo0009

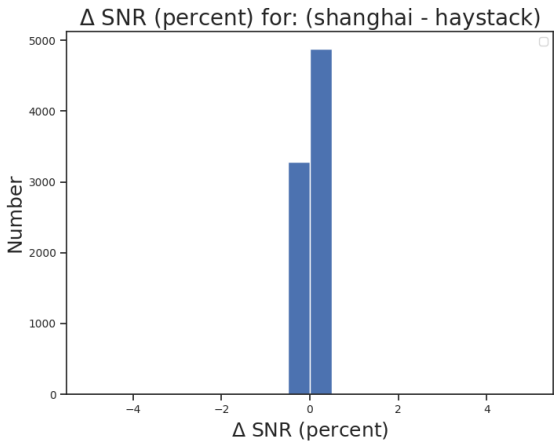

(a) Distribution of the difference in scan SNR

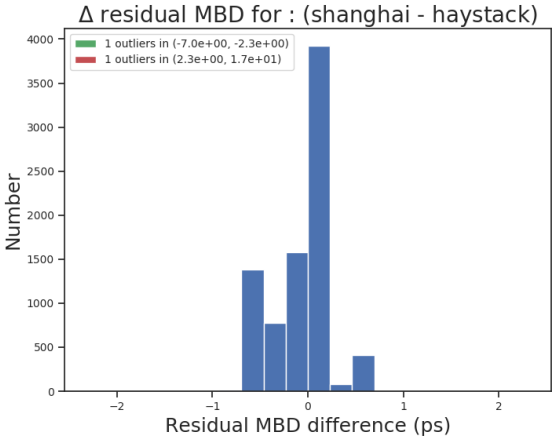

(b) Distribution of the difference in residual multi-band delay

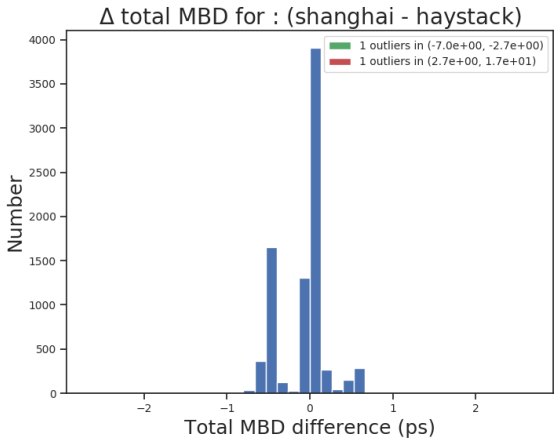

(c) Distribution of the difference in the total multi-band delay

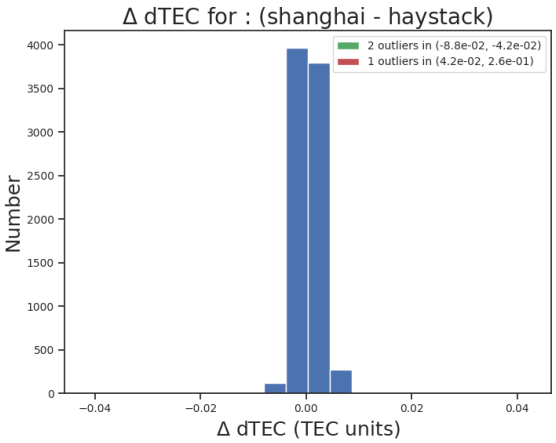

(d) Distribution of the difference in the scan dTEC

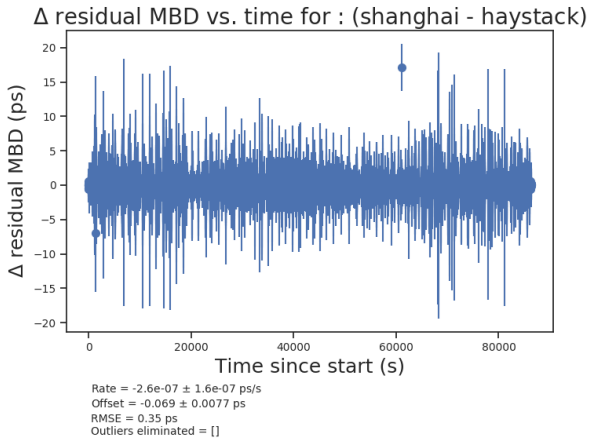

(e) Difference in the residual multi-band delay as a function of time since start, error bars are the formal MBD error reported by fourfit.

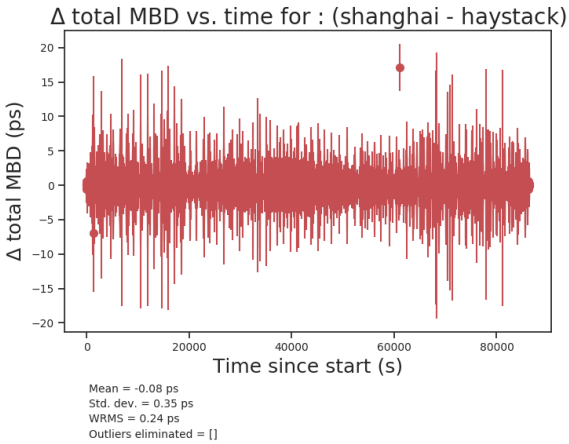

(f) Difference in the total multi-band delay as a function of time since start, error bars are the formal MBD error reported by fourfit.

Figure 11: Comparison of Shanghai scan parameters with Haystack for vo0009

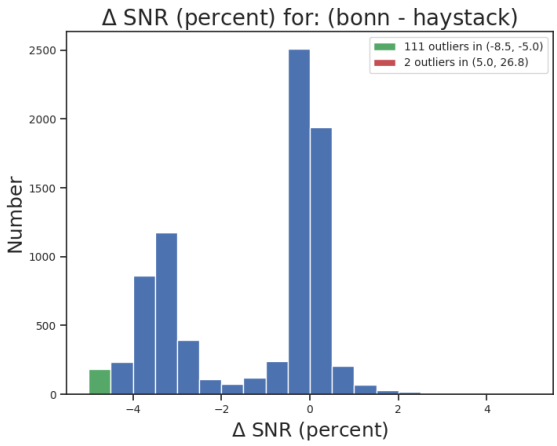

(a) Distribution of the difference in scan SNR

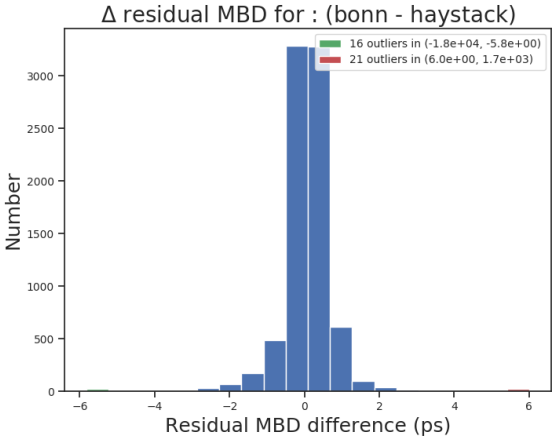

(b) Distribution of the difference in residual multi-band delay

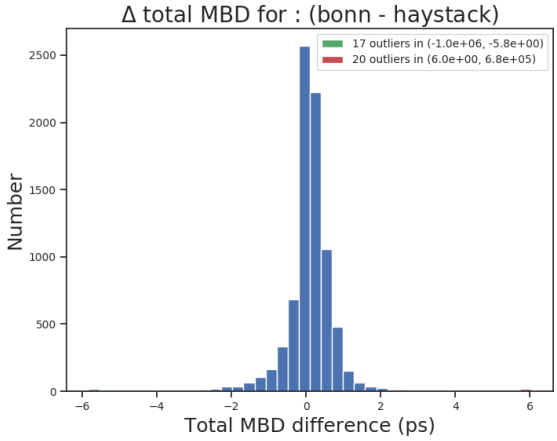

(c) Distribution of the difference in the total multi-band delay

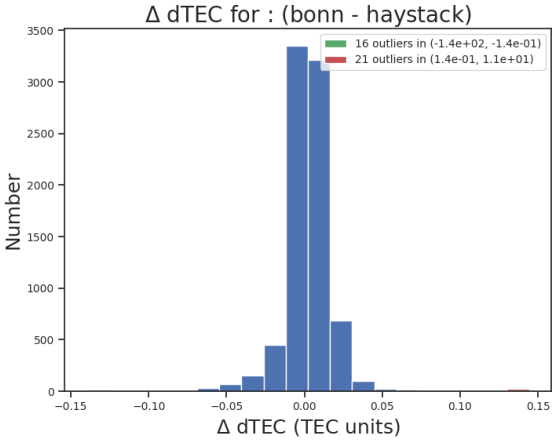

(d) Distribution of the difference in the scan dTEC

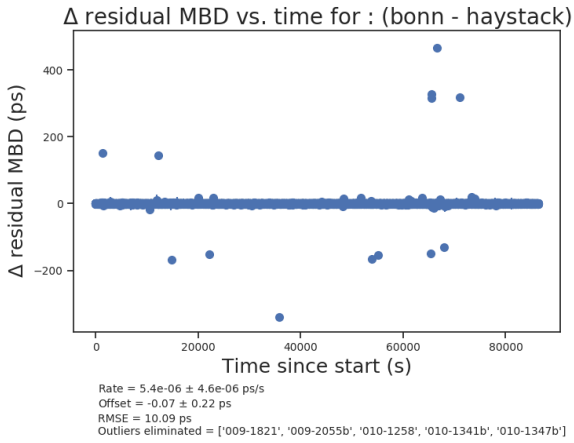

(e) Difference in the residual multi-band delay as a function of time since start, error bars are the formal MBD error reported by fourfit.

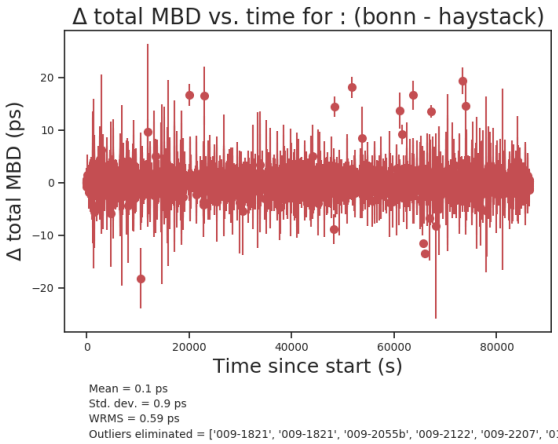

(f) Difference in the total multi-band delay as a function of time since start, error bars are the formal MBD error reported by fourfit.

Figure 12: Comparison of Bonn scan parameters with Haystack for vo0009

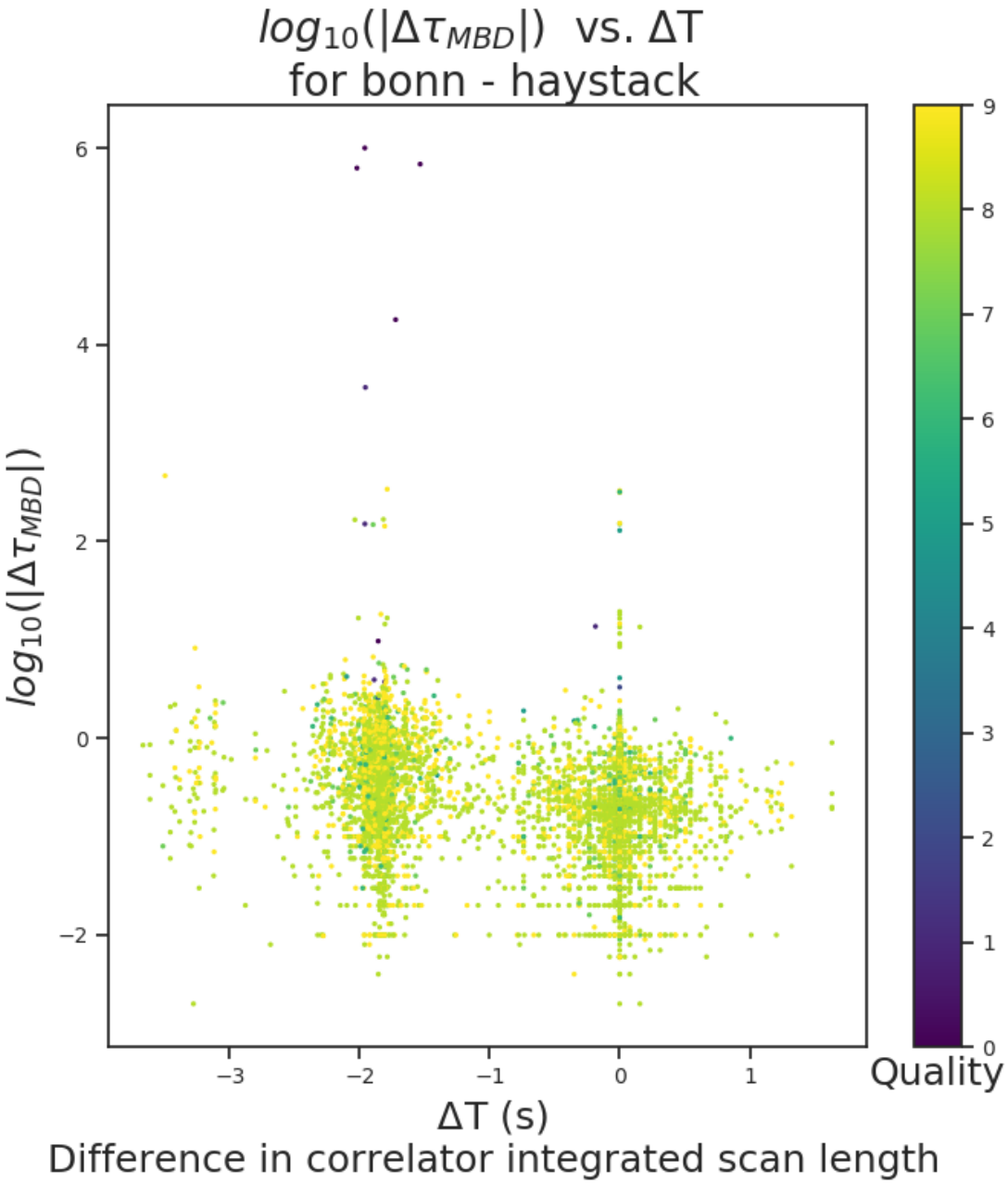

Figure 13: Plot of the log of the total multi-band delay difference ($\Delta\tau_{MBD}$) as a function of the difference in the correlator integration time (ΔT). The color scale represent the quality-code (0-9) of the scan. Note that the scatter does not exhibit a strong correlation between the value of ΔT and $\Delta\tau_{MBD}$, but also that some of the lowest quality scans (Q=0) exhibit the largest $\Delta\tau_{MBD}$. Also note the cluster of scans near $\Delta T = 1.8$ seconds (which is approximately 1/16 of the length of a typical scan), we suspect that this coincides with the failure to mount/read one disk in the two-module (16) disk pack associated with GGAO12M.

scan (category)	baseline	source	quality code (Haystack)	quality code (Bonn)	SNR (Haystack)	SNR (Bonn)	$\Delta\tau_{MBD}$ (ps)	ΔdTEC (TECU)	ΔT (s)
009-1821 (2)	GS	1806+456	1G	1G	223.92	213.32	150.8	2.17	-1.96
009-1821 (2)	GT	1806+456	1G	1G	173.92	161.43	-3679.7	-22.78	-1.96
010-0010	IE	3C418	7	7	106.26	107.3	-151.07	-7.1	0.0
010-1209	GI	3C418	7	7	90.85	87.22	-148.27	-7.02	-1.9
010-1252 (2)	IS	3C418	5G	5G	144.15	142.95	-129.4	-6.68	0.0
009-2122	GI	0642+449	8	9	30.27	29.74	143.22	6.91	-1.81
009-2207	GI	0642+449	8	8	29.44	28.29	-167.78	2.54	-1.82
010-0857	GI	0642+449	8	8	38.7	37.42	-166.04	2.6	-2.04
010-0918a	IE	0642+449	9	9	37.9	38.6	-153.2	-7.14	0.0
010-1229a	GE	1406-076	9	9	17.06	16.38	465.59	11.26	-3.5
010-1258 (1)	GE	1406-076	0	0	5.77	5.87	-624174.47	3.13	-2.02
010-1347b (1)	GE	1406-076	0	0	6.09	6.17	-17945.8	-140.47	-1.72
010-1212	IE	1418+546	9	9	23.97	23.9	314.8	4.58	0.0
010-1212	IT	1418+546	9	9	27.72	27.77	328.3	4.86	0.0
010-0356	GV	1418+546	9	9	51.07	50.65	-339.8	-5.09	-1.79
009-2055b (1)	GE	2227-088	0	0	6.75	6.52	684321.07	-53.02	-1.53
010-1341b (1)	GE	1213-172	0	0	6.72	6.82	-998280.21	-69.02	-1.96
010-1343	IV	0229+131	6	6	68.53	68.56	318.6	4.61	0.0

Table 3: Table of scans which are considered extreme outliers since they exhibit a modified z-score[2] associated with a total multi-band delay differences ($\Delta\tau_{MBD}$) that is larger than 100. Scans for which a reason for the discrepancy is readily apparent are labeled with a category in the first column. The two categories are (1) Non-detection and/or zero-fringe rate, and (2) error code 'G' which indicates that the power is lower than expected in one or several channels.

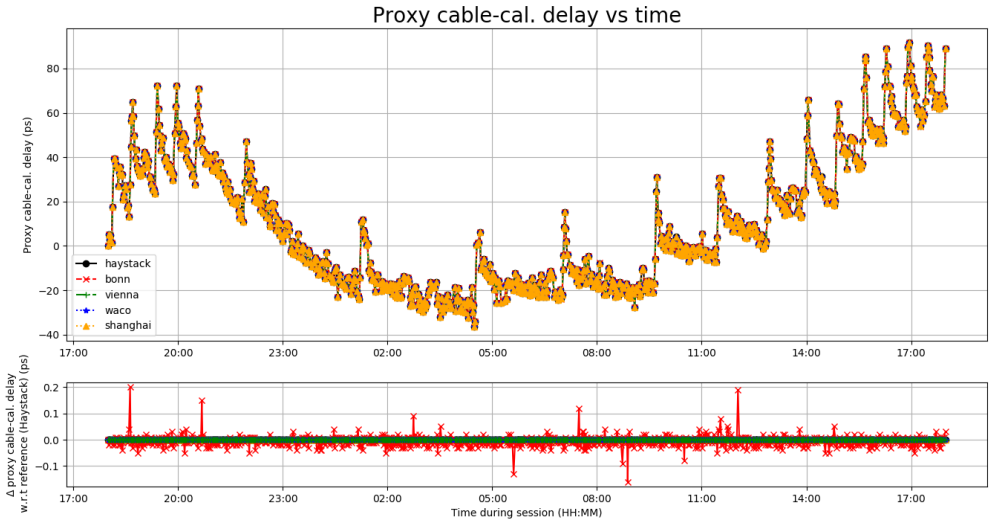

Figure 14: The proxy cable-cal delay computed by each correlator for GGAO12M (G) as a function of time during vo0009.

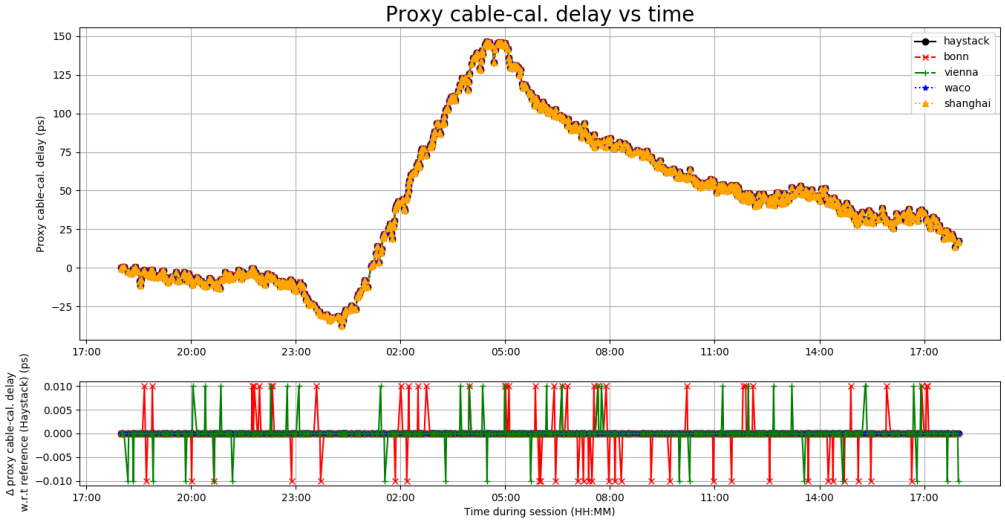

Figure 15: The proxy cable-cal delay computed by each correlator for Ishioka (I) as a function of time during vo0009.

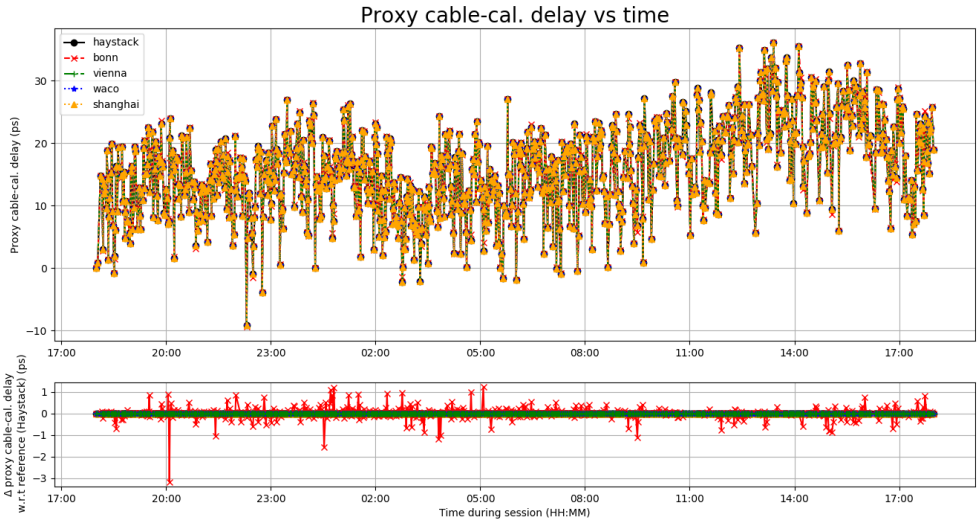

Figure 16: The proxy cable-cal delay computed by each correlator for Wettzell (Ws) as a function of time during vo0009.